Results in Physics 42 (2022) 105985

Contents lists available at ScienceDirect

Results in Physics

journal homepage: www.elsevier.com/locate/rinp

Beam-distortion enhanced terahertz radiation generation in air

V. Vaičaitis *, V. Tamulienė

Laser Research Center, Vilnius University, Saulėtekio 10, Vilnius LT-10223, Lithuania

ARTICLE INFO

Keywords:
Femtosecond laser
Bichromatic pump
Terahertz radiation
Plasma

ABSTRACT

Here we for the first time report an enhancement of terahertz (THz) radiation generation in air by a partial blocking of bichromatic pump beam consisting of the femtosecond Ti:Sapphire laser fundamental and its second harmonic. Both the experimental results and numerical analysis of the generation process demonstrated an increase of THz radiation yield by 15–20 percent over a wide range of the pump power and other experimental parameters. The dominant mechanism of THz radiation generation enhancement was found to be the pump pulse splitting suppression during its propagation in the plasma channel induced by the distorted beam.

Introduction

Terahertz (THz) radiation generation in air by focused bichromatic femtosecond laser pulses [1,2], allows to obtain very high THz field strengths and extremely broadband spectral widths [3–6]. However, in most experiments the simple set-up based on the fundamental and its second harmonic (FH and SH, respectively) of Ti:sapphire laser has been used as a pump source, which resulted in a quite low generation efficiency, typically not exceeding $10^{-4}-10^{-3}$ [5,7–9]. Therefore, many sophisticated methods have been proposed to solve this problem. Thus, the use of longer wavelength femtosecond laser pulses showed a strong wavelength scaling of THz generation efficiency [10–13]. In addition, there were reported both the experimental and theoretical findings on THz generation by two-color laser pulses with uncommon frequency ratios [14–18] as well as by three-color [17,19–21] or even multicolor pump pulses [22]. Also, it was demonstrated [2,23,24] that the circularly polarized FH and SH pulses produce a significantly (by a factor of up to 8) higher THz yield in comparison with the linearly polarized ones. However, the above mentioned methods to increase THz yield usually require specific and complex set-ups, which can make their practical implementation quite difficult and time consuming. On the other hand, it is commonly known that the source of THz radiation in air plasma, created by bichromatic laser pulses are the microcurrents induced by asymmetric pump fields. Therefore it is naturally to expect that in presence of preexisting plasma THz generation efficiency could increase, in a way similar to that, for example, of third harmonic generation [25]. However, in contrast to the expectations there are many reports, indicating that under such conditions the efficiency of THz generation significantly (up to 60 percent [26–29]) decreases. The only exception is the case when two plasma filaments created by the separate laser pulses are concatenated, which results in an increase of THz generation efficiency due to artificially prolonged plasma filament [30]. Thus, the modification of the plasma filament parameters (plasma density, spatial and temporal distribution, etc.) may significantly affect THz generation in the plasma. Therefore in this paper we for the first time demonstrate both experimentally and numerically the increase of THz radiation yield due to the partial pump beam blocking. Note that though the THz radiation yield is enhanced the plasma density as well as the pump intensity in the filament decrease under these conditions. We show that the origin of this counterintuitive phenomenon is the suppression of the pump pulse splitting during propagation in the plasma when the beam is distorted and becomes asymmetric. Although there exist other more efficient methods to enhance the THz generation the reported method of cutting the pump beam with a knife is quite simple since it does not require scaling of neither laser power nor pump wavelength.

Experimental

As a source of femtosecond laser pulses a 1 kHz repetition rate Ti:sapphire laser system (Legend elite duo HE+, Coherent Inc.) was used. Laser pulse duration was 35–40 fs (FWHM), its central wavelength was about 790 nm and a maximal available pulse energy of 5 mJ could be varied with the help of an optical attenuator (a zero-order half-wave plate and a thin polarizer). The laser pulses were focused in air by a lens with the focal length of 50 cm through a 0.2 mm-thick nonlinear BBO crystal (type I, cut angles: $\theta \approx 29°$ and $\varphi \approx 90°$). As a result, the pump beam consisted of the FH and SH waves and produced a plasma filament, where THz radiation was generated. While the location of SH crystal with respect to the plasma filament could be tuned during the experiment, its azimuthal angle was set at the point of maximal THz

* Corresponding author.
E-mail address: Virgilijus.Vaicaitis@ff.vu.lt (V. Vaičaitis).

https://doi.org/10.1016/j.rinp.2022.105985
Received 30 May 2022; Received in revised form 7 September 2022; Accepted 9 September 2022
Available online 14 September 2022

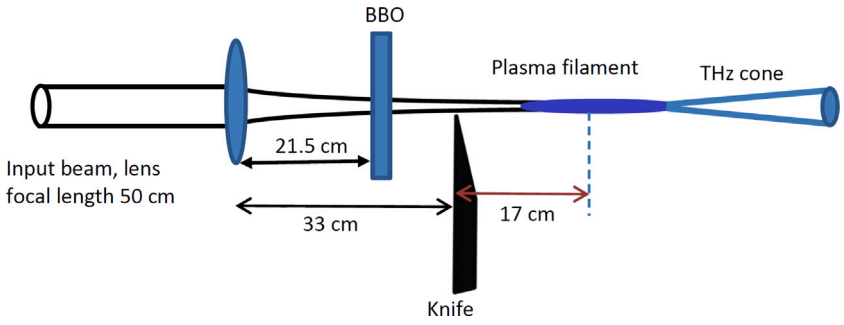

Fig. 1. Experimental setup.

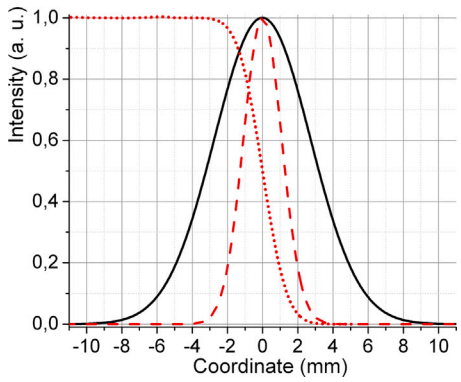

Fig. 2. Laser beam intensity profile (red dashed line) near the knife edge and (black solid line) just before the focusing lens. Red dotted line represents the pump beam power as a function of knife edge position. (For interpretation of the references to color in this figure legend, the reader is referred to the web version of this article.)

radiation generation efficiency [3,31]. At about 33 cm from the lens a part of the focused beam could be fully or partially blocked by the edge of a metallic knife (Fig. 1). Near the knife edge the laser beam diameter was about 2.6 mm (FWHM), while at the input of focusing lens it was about 6.4 mm (Fig. 2).

A calibrated pyroelectric detector (TPR-A-65 THz, Spectrum Detector Inc.) was used for power measurements of generated THz radiation. In order to increase its sensitivity and signal to noise ratio the pump beam was modulated by a mechanical beam chopper (modulation rate 5 Hz), synchronized with a computer-controlled lock-in amplifier. Both the knife and nonlinear BBO crystal were placed on the computer-controlled translation stages, thus, most of the measurements were automated during the experiment.

By using a well-known knife edge (Razor-blade) technique [32–34] we have measured the power of transmitted beam as a function of knife edge position across the beam. A plot of these data shows a characteristic S-shaped curve of the error function decreasing from the total beam power to zero (Fig. 2). Note that first derivative of this function yields beam intensity distribution shown by the solid and dashed lines.

Numerical

The model. The numerical simulation is based on the model presented in [35]. The main difference is the absence of the cylindrical symmetry in the present simulations. Therefore, fast Fourier transform instead of the Hankel transform was performed. The boundary conditions differ as well. However, the model equation is the same as in [35], so we refer to this cited work for the detailed description of the equation terms (Eq. (1) below). The governing equation of the unidirectional propagation was written for the Fourier transform $\hat{\mathcal{E}}(\omega, \beta_x, \beta_y, z)$ of the analytical signal $\mathcal{E}(t, x, y, z)$:

$$\frac{\partial \hat{\mathcal{E}}}{\partial z} = iK_z\hat{\mathcal{E}} + i\hat{P}_{Kerr} - i\hat{P}_{pl} - \hat{P}_{loss}. \tag{1}$$

Here, t is time and x, y, z are the Cartesian coordinates. The electric field $E = \mathrm{Re}(\mathcal{E})$, where $\mathrm{Re}(\circ)$ denotes the real part. The first rhs. term $iK_z\hat{\mathcal{E}}$ is the linear propagation term which includes the time walk-off and higher dispersion terms as well as beam diffraction. The second rhs. term $i\hat{P}_{Kerr}$ describes the third-order nonlinearity of air. Third and fourth rhs. terms $-i\hat{P}_{pl}$ and $-\hat{P}_{loss}$ are the plasma and nonlinear losses terms, respectively. These two last terms require an additional equation for the plasma density. As in [35], we utilize Yudin–Ivanov formula [36] of the plasma generation, see also Eq. (15) in [37].

Input waves. At $z = 0$ the input analytical signal of FH is given by

$$\mathcal{E}(t, x, y, z = 0) = E_0 \exp\left(-(x^2 + y^2)\left[\frac{1}{r_{10}^2} + \frac{i\pi}{\lambda_{10} f}\right] - 2\log(2)\frac{t^2}{\tau^2} - i\omega_{10}t\right). \tag{2}$$

This is a beam focused by a lens of the focus length f. τ is the pulse duration at FWHM. r_{10}, λ_{10} and ω_{10} are the FH beam radius, wavelength and angular frequency, respectively. E_0 is the input amplitude.

The propagation of the FH from lens to BBO crystal (distance L_0) was calculated without inclusion of nonlinear and plasma terms. Here, the linear propagation equation was solved. At BBO crystal, the SH was generated:

$$\mathcal{E}(t, x, y, z = L_0) = \mathcal{E}_1(t, x, y, z = L_0) + \frac{a_m}{\max(\mathcal{E}_1)}\mathcal{E}_1^2(t, x, y, z = L_0), \tag{3}$$

where E_1 is the analytical signal of FH and a_m is the fraction of the SH and FH amplitudes.

At $z = L_0$ the nonlinear and plasma terms start to be included. At $z = L_0 + L_k$ the beam is cut by a knife, Fig. 1. The knife direction is the x-axis direction. Then, the propagation to the lens focus is simulated.

Parameters. Eq. (1) was simulated by the use of the symmetrized split-step Fourier transform method [38]. The longitudinal step h_z was different: at $L_0 \le z < L_0 + L_k$, $h_z = (f - L_0)/n_z$, where $n_z = 120$. Then, at $z \ge L_0 + L_k$, $h_z = (f - L_0)/(80 \times n_z)$. In the time and space domains, a fast Fourier transform was used. The domain of the (x, y) coordinates $2r_{10} \le x, y < 2r_{10}$ was divided into 128 equal steps and the time domain $t \in [-2.5\tau,\ 2.5\tau)$ was divided into 1024 equal steps. The parameters: $\lambda_{10} = 790$ nm, $f = 50$ cm, $L_0 = 20$ cm, $L_k = 13$ cm, $2r_{10} = 3$ mm, $\tau = 40$ fs. Input FH energy was 100 μJ and fraction $a_m^2 = 0.01$.

Results and discussion

In the experiment, using the set-up described above we have measured THz power dependence on the knife edge position. Surprisingly, in contrast to the transmitted beam power, by moving the knife edge, the power of THz radiation first increased by up to 20% and only then

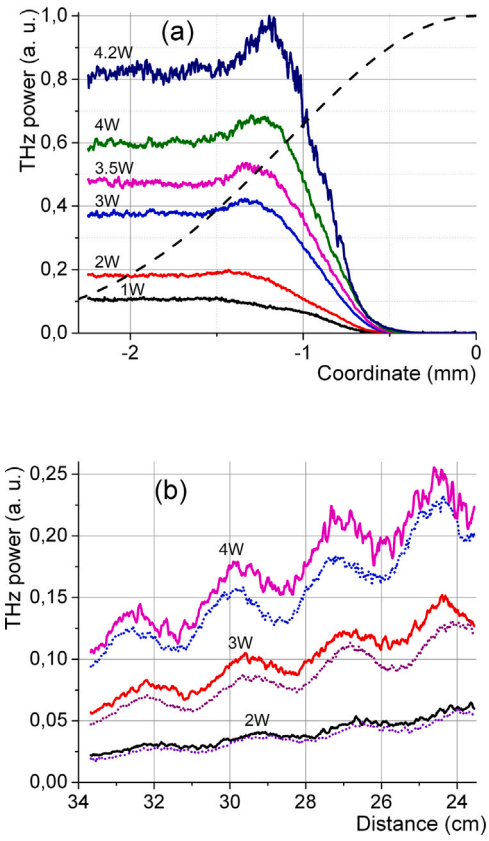

Fig. 3. Dependences of THz power as a function of (a) the knife edge position for various pump powers and (b) the distance between the nonlinear BBO crystal and plasma filament (solid lines represent the case of unperturbed beam, while the dotted lines show the corresponding data when the beam was partially blocked). Black dashed line in (a) represents the pump beam intensity, corresponding to the knife edge coordinate (beam radius). Experimental results.

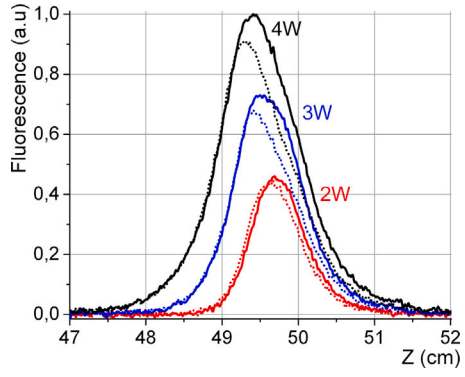

Fig. 4. Plasma fluorescence intensity in the filament as a function of coordinate along the optical axis for the pump power of 2, 3 and 4 W. Solid lines represent fluorescence of the filament created by the non-truncated beam, while dashed curves represent fluorescence from the filament created by the partially blocked beam. Experimental results.

decreased to zero (Fig. 3a). The similar knife-induced increase of THz power has been observed for various pump beam powers and distances between the air plasma filament and nonlinear second harmonic crystal (Fig. 3b).

Note that the knife position at which the maximal THz generation efficiency took place was clearly dependent on the pump power: for the pump power of about 4.2 W the maximal increase of THz power has been observed, when the knife was positioned at about 1.2 mm from the

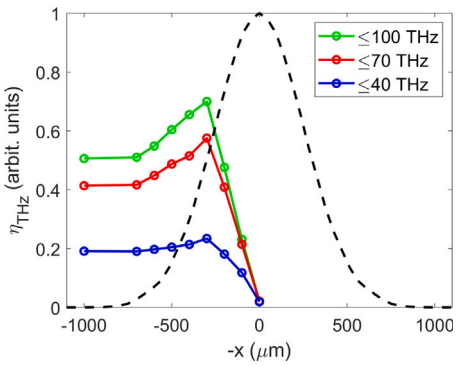

Fig. 5. Dependences of THz efficiency on the knife position (solid lines). THz efficiency was calculated at $\nu \leq 40$ THz, $\nu \leq 70$ THz and $\nu \leq 100$ THz. Dashed line: beam profile before cutting. Numerical results.

beam axis, while for the pump power of about 2 W the optimal position of the knife edge was a little less than 1.4 mm, which corresponds to the 54 and 44 percent of maximal beam intensity, respectively. Thus, for the higher pump powers the larger portion of the beam had to be blocked in order to get the maximal increase of THz generation efficiency. In addition note that the increase of THz yield was larger for the higher pump powers, which indicates the nonlinear nature of this phenomenon. Therefore, we have also compared plasma filaments created by the truncated and non-truncated laser beams. While it was quite difficult to study their differences by a naked eye, the plasma fluorescence, captured by a CCD camera revealed some interesting features (Fig. 4). Thus, the beam truncation resulted in some decrease of the fluorescence at the trailing edge of the filament, which indicates that the plasma density slightly decreased along with the decrease of the overall filament length. This result is somewhat counterintuitive, since as it was mentioned above, a strong increase of THz generation efficiency in artificially prolonged plasma filaments has been reported in [30]. On the other hand, recently under the similar experimental conditions we have demonstrated a white-light supercontinuum generation enhancement, which has been interpreted as a result of diffraction-induced laser beam intensity modifications [39].

The numerically obtained dependences of THz efficiency on the knife position are presented in Fig. 5. As in experiment, the THz efficiency is enhanced when the beam blocking is applied. The strongest effect is seen at $x = 300$ μm. This value is smaller than the experimental one (Fig. 3a) since in the numerical simulations the size of the input beam was taken smaller in order to save the computational time. However, the knife position corresponds to around 60 percent of maximal beam intensity which is in good qualitative agreement with the experiment.

In Fig. 6, the numerical evolutions of THz generation efficiencies, plasma densities and beam intensities during the propagation are compared for optimally blocked and not blocked pump beams. One can see that THz efficiency saturates at $z > f = 50$ cm. Although the partially blocked beam yields higher output THz yield, the plasma density is lower compared to the undisturbed beam, Fig. 6b. This finding is in agreement with the experimentally registered fluorescence, Fig. 4. The light intensity becomes lower as well, Fig. 6c.

Another interesting finding can be seen in Fig. 7. When the pump beams are distorted, the THz spectrum is modified: it becomes broader. Since in the experiment THz spectrum has spanned up to 70 THz, this broadening made influence to the registered efficiency. The effect becomes weaker when the integration up to 40 THz is applied, compare red and blue solid lines in Fig. 5.

An explanation of the findings discussed above can be given by comparing pulse propagation evolutions of undistorted and partially blocked pump beams. Typically, the pump pulse splits into two pulses

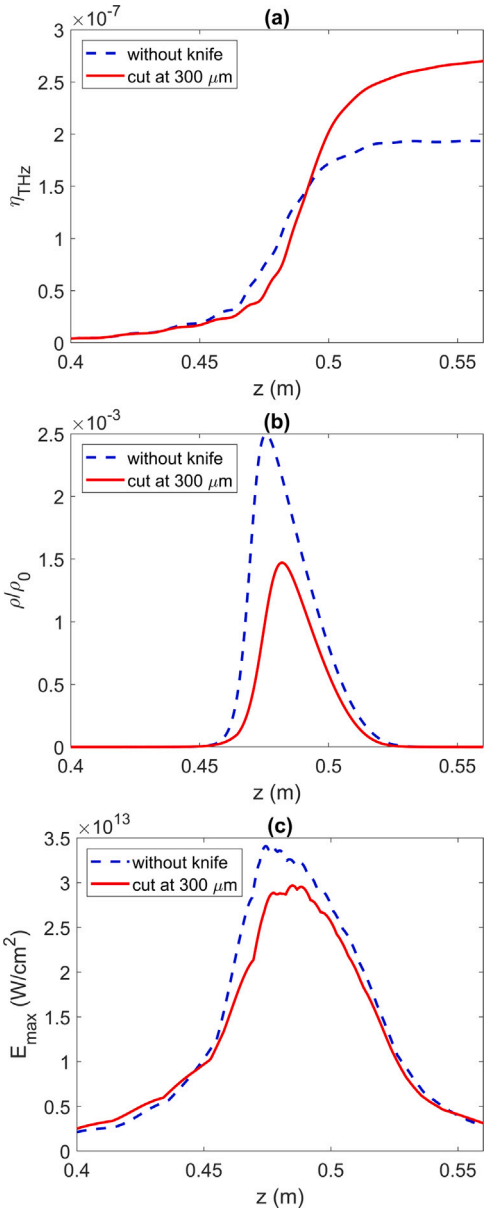

Fig. 6. Dependences of THz efficiency (a), plasma density (b) and maximum intensity (c) on propagation distance. No cutting (blue dashed lines) and knife at $x = 300$ μm (red solid lines) applied. Numerical results. (For interpretation of the references to color in this figure legend, the reader is referred to the web version of this article.)

due to the beam tail refocusing [40] and this pulse splitting is observed for the undistorted beam, left panel of Fig. 8. However, the distorted beam keeps localized structure (Fig. 8 right panel) and although its maximum intensity is slightly lower than that of the undistorted beam (Fig. 6c), the pulse is more localized in time domain. Specifically, since the pump beam was distorted by a knife, the refocusing process meets obstacles: the beam is not symmetric and the intensity is lower. As a result, the generated THz pulse is more localized in time domain as well, Fig. 9. Then, the THz pulse obtains higher intensity (Fig. 9) and broader spectrum (Fig. 7), and as a result the overall THz generation efficiency is enhanced.

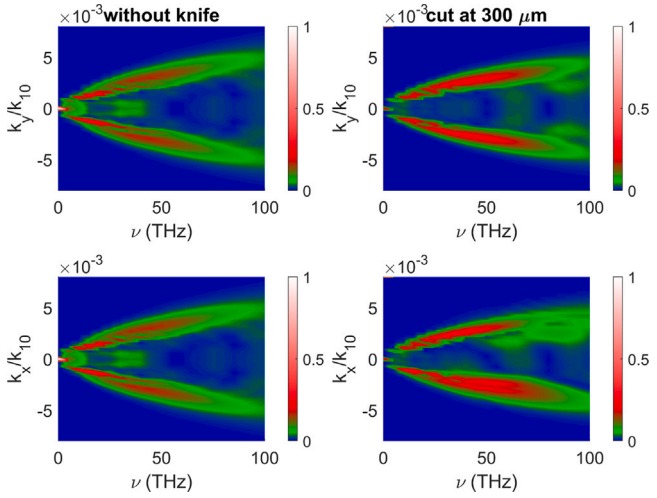

Fig. 7. THz spectrum amplitude profiles at the output. No cutting (left) and optimal cutting at 300 μm (right) applied. x (bottom) and y (top) projections are presented. Numerical results.

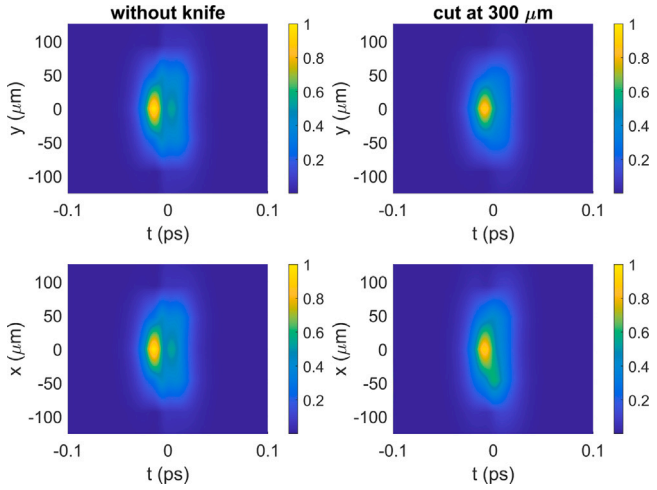

Fig. 8. FH intensity distributions at the vicinity of the lens focus ($z = 48.6$ cm). No cutting (left) and optimal cutting at 300 μm (right) applied. x (bottom) and y (top) projections are presented. Numerical results.

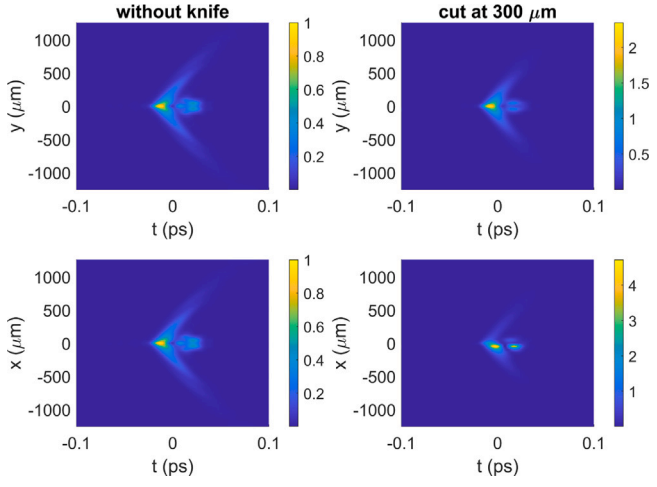

Fig. 9. THz intensity distributions at the vicinity of the lens focus ($z = 48.6$ cm). No cutting (left) and optimal cutting at 300 μm (right) applied. x (bottom) and y (top) projections are presented. Numerical results.

Conclusions

In conclusion, we have demonstrated, for the first time, a beam-distortion enhanced THz radiation generation in air by focused femtosecond laser pulses. The numerical modeling based on an analysis of a unidirectional pulse propagation equation showed a good qualitatively agreement between the experimental and numerical results. The explanation of the THz efficiency enhancement based on the analysis of the pump pulse propagation in plasma channel is provided. The power of THz radiation is enhanced due to the suppression of the pump pulse splitting that is caused by the suppressed refocusing when the beam is cut with a knife. As a result, the pump pulse becomes shorter and more localized in time domain, therefore generated THz pulse is shorter and more intense, and its spectrum is broader. This raises the output THz power. Though increase of THz radiation generation efficiency in the filament created by partially blocked bichromatic pump beam was only 15–20 percent higher than that obtained from a simply focused beam, apart from the scientific importance this effect also could find practical applications, whenever the laser power scaling is not available or limited.

CRediT authorship contribution statement

V. Vaičaitis: Conceptualization, Methodology, Writing – original draft, Experimental investigation. **V. Tamulienė:** Conceptualization, Methodology, Software, Writing – original draft, Numerical investigation.

Declaration of competing interest

The authors declare that they have no known competing financial interests or personal relationships that could have appeared to influence the work reported in this paper.

Data availability

Data will be made available on request.

References

[1] Cook DJ, Hochstrasser RM. Intense terahertz pulses by four-wave rectification in air. Opt Lett 2000;25(16):1210—1212. http://dx.doi.org/10.1364/OL.25.001210.

[2] Tailliez C, Stathopulos A, Skupin S, Buožius D, Babushkin I, Vaičaitis V, et al. Terahertz pulse generation by two-color laser fields with circular polarization. New J Phys 2020;22(10):103038. http://dx.doi.org/10.1088/1367-2630/abb863.

[3] Kim KY, Taylor AJ, Glownia JH, Rodriguez G. Coherent control of terahertz supercontinuum generation in ultrafast laser-gas interactions. Nat Photonics 2008;2:605–9. http://dx.doi.org/10.1038/nphoton.2008.153.

[4] Ivanov M, Thiele I, Bergé L, Skupin S, Buožius D, Vaičaitis V. Intensity modulated terahertz vortex wave generation in air plasma by two-color femtosecond laser pulses. Opt Lett 2019;44(15):3889–92. http://dx.doi.org/10.1364/OL.44.003889.

[5] Oh TI, Yoo YJ, You YS, Kim KY. Generation of strong terahertz fields exceeding 8 MV/cm at 1 kHz and real-time beam profiling. Appl Phys Lett 2014;105(4):041103. http://dx.doi.org/10.1063/1.4891678.

[6] Prost E, Loriot V, Constant E, Compagnon I, Bergé L, Lépine F, et al. Air-photonics terahertz platform with versatile micro-controller based interface and data acquisition. Rev Sci Instrum 2022;93(3):033004. http://dx.doi.org/10.1063/5.0082593.

[7] Yoo Y-J, Kuk D, Zhong Z, Kim K-Y. Generation and characterization of strong terahertz fields from kHz laser filamentation. IEEE J Sel Top Quantum Electron 2017;23(4):8501007. http://dx.doi.org/10.1109/JSTQE.2016.2644259.

[8] Minami Y, Kurihara T, Yamaguchi K, Nakajima M, Suemoto T. High-power THz wave generation in plasma induced by polarization adjusted two-color laser pulses. Appl Phys Lett 2013;102(4):041105. http://dx.doi.org/10.1063/1.4789773.

[9] Sun WF, Wang XK, Zhang Y. Terahertz generation from laser-induced plasma. Opto-Electron Sci 2022;1(8):220003. http://dx.doi.org/10.29026/oes.2022.220003.

[10] Wang W-M, Kawata S, Sheng Z-M, Li Y-T, Chen L-M, Qian L-J, et al. Efficient terahertz emission by mid-infrared laser pulses from gas targets. Opt Lett 2011;36(14):2608–10. http://dx.doi.org/10.1364/OL.36.002608.

[11] Clerici M, Peccianti M, Schmidt BE, Caspani L, Shalaby M, Gigu'ere M, et al. Wavelength scaling of terahertz generation by gas ionization. Phys Rev Lett 2013;110(25):253901. http://dx.doi.org/10.1103/PhysRevLett.110.253901.

[12] Koulouklidis AD, Gollner C, Shumakova V, Fedorov V Yu, Pugžlys A, Baltuška A, et al. Observation of extremely efficient terahertz generation from mid-infrared two-color laser filaments. Nature Commun 2020;11:292. http://dx.doi.org/10.1038/s41467-019-14206-x.

[13] Wang G-L, Qi H-X, Li Y-N, Jiao Z-H, Zhao S-F, Zhang L. Polarization-controlled terahertz generation by bicircular longer-wavelength laser fields. J Opt Soc Amer B 2022;39(5):1370–7. http://dx.doi.org/10.1364/JOSAB.456066.

[14] Thomson MD, Blank V, Roskos HG. Terahertz white-light pulses from an air plasma photo-induced by incommensurate two-color optical fields. Opt Express 2010;18(22):23173–82. http://dx.doi.org/10.1364/OE.18.023173.

[15] Vvedenskii NV, Korytin AI, Kostin VA, Murzanev AA, Silaev AA, Stepanov AN. Two-color laser-plasma generation of terahertz radiation using a frequency-tunable half harmonic of a femtosecond pulse. Phys Rev Lett 2014;112(5):055004. http://dx.doi.org/10.1103/PhysRevLett.112.055004.

[16] Balčiūnas T, Lorenc D, Ivanov M, Smirnova O, Zheltikov AM, Dietze D, et al. CEP-stable tunable THz-emission originating from laser-waveform-controlled sub-cycle plasma-electron bursts. Opt Express 2015;23(12):15278–89. http://dx.doi.org/10.1364/OE.23.015278.

[17] Bagley JD, Moss CD, Sorenson SA, Johnson JA. Laser-induced plasma generation of terahertz radiation using three incommensurate wavelengths. J Phys B: At Mol Opt Phys 2018;51(14):144004. http://dx.doi.org/10.1088/1361-6455/aac6ef.

[18] Fan Z, Lu C, Liu Y. Tunable broadband THz emission from air plasma pumped by femtosecond pulses composed of a fundamental frequency with its detuned second harmonic. Opt Commun 2022;505:127532. http://dx.doi.org/10.1016/j.optcom.2021.127532.

[19] Vaičaitis V, Balachninaitė O, Morgner U, Babushkin I. Terahertz radiation generation by three-color laser pulses in air filament. J Appl Phys 2019;125(17):173103. http://dx.doi.org/10.1063/1.5078683.

[20] Ma D, Dong L, Zhang M, Wu T, Zhao Y, Zhang L, et al. Enhancement of terahertz waves from two-color laser-field induced air plasma excited using a third-color femtosecond laser. Opt Express 2020;28(14):20598–608. http://dx.doi.org/10.1364/OE.395130.

[21] Ma D, Dong L, Zhang R, Zhang C, Zhao Y, Zhang L. Enhancement of terahertz wave emission from air plasma excited by harmonic three-color laser fields. Opt Commun 2021;481(15):12653. http://dx.doi.org/10.1016/j.optcom.2020.126533.

[22] de Alaiza Martínez PG, Babushkin I, Bergé L, Skupin S, Cabrera-Granado E, Köhler C, et al. Boosting terahertz generation in laser-field ionized gases using a sawtooth wave shape. Phys Rev Lett 2015;114(18):183901. http://dx.doi.org/10.1103/PhysRevLett.114.183901.

[23] Meng C, Chen W, Wang X, Lü Z, Huang Y, Liu J, et al. Enhancement of terahertz radiation by using circularly polarized two-color laser fields. Appl Phys Lett 2016;109(13):131105. http://dx.doi.org/10.1063/1.4963883.

[24] Tu Y-Y, Meng C, Sun X, Wu H-Z, Song P, Meng C-S, et al. Enhancement of terahertz radiation from a filament by using circularly polarized two-color laser fields. J Opt Soc Amer B 2022;39(3):A83–8. http://dx.doi.org/10.1364/JOSAB.446156.

[25] Suntsov S, Abdollahpour D, Papazoglou DG, Tzortzakis S. Efficient third-harmonic generation through tailored IR femtosecond laser pulse filamentation in air. Opt Express 2009;17(5):3190–5. http://dx.doi.org/10.1364/OE.17.003190.

[26] Wen H, Daranciang D, Lindenberg AM. High-speed all-optical terahertz polarization switching by a transient plasma phase modulator. Appl Phys Lett 2010;96(15):161103. http://dx.doi.org/10.1063/1.3407514.

[27] Minami Y, Nakajima M, Suemoto T. Effect of preformed plasma on terahertz-wave emission from the plasma generated by two-color laser pulses. Phys Rev A 2011;83(2):023828. http://dx.doi.org/10.1103/PhysRevA.83.023828.

[28] Das J, Yamaguchi M. Terahertz wave excitation from preexisting air plasma. J Opt Soc Amer B 2013;30(6):1595–600. http://dx.doi.org/10.1364/JOSAB.30.001595.

[29] Vaičaitis V, Ivanov M, Adomavičius K, Svirskas Ž, Morgner U, Babushkin I. Influence of laser-preformed plasma on THz wave generation in air by bichromatic laser pulses. Laser Phys 2018;28(9):095402. http://dx.doi.org/10.1088/1555-6611/aaca5f.

[30] Manceau J-M, Massaouti M, Tzortzakis S. Strong terahertz emission enhancement via femtosecond laser filament concatenation in air. Opt Lett 2010;35(14):2424–6. http://dx.doi.org/10.1364/OL.35.002424.

[31] Pyragaitė V, Smilgevičius V, Steponkevičius K, Makauskas B, Vaičaitis V. Phase shifts in terahertz wave generation by tightly focused bichromatic laser pulses. J Opt Soc Amer B 2014;31(7):1430–5. http://dx.doi.org/10.1364/JOSAB.31.001430.

[32] Suzaki Y, Tachibana A. Measurement of the μm sized radius of Gaussian laser beam using the scanning knife-edge. Appl Opt 1975;14(12):2809–10. http://dx.doi.org/10.1364/AO.14.002809.

[33] González-Cardel M, Arguijo P, Díaz-Uribe R. Gaussian beam radius measurement with a knife-edge: a polynomial approximation to the inverse error function. Appl Opt 2013;52(16):3849–55. http://dx.doi.org/10.1364/AO.52.003849.

[34] Khosrofian JM, Garetz BA. Measurement of a Gaussian laser beam diameter through the direct inversion of knife-edge data. Appl Opt 1983;22(21):3406–10. http://dx.doi.org/10.1364/AO.22.003406.

[35] Buožius D, Motiejūnas B, Vaičaitis V, Tamulienė V. Emission of conical THz radiation induced by bichromatic pump X waves in an air plasma. Phys Rev A 2022;105(2):023521. http://dx.doi.org/10.1103/PhysRevA.105.023521.

[36] Yudin GL, Ivanov MY. Nonadiabatic tunnel ionization: looking inside a laser cycle. Phys Rev A 2001;64(1):013409. http://dx.doi.org/10.1103/PhysRevA.64.013409.

[37] Tamulienė V, Juškevičiūtė G, Buožius D, Vaičaitis V, Babushkin I, Morgner U. Influence of tunnel ionization to third-harmonic generation of infrared femtosecond laser pulses in air. Sci Rep 2020;10:17437. http://dx.doi.org/10.1038/s41598-020-74263-x.

[38] Wartak MS. Computational photonics. An introduction with MATLAB. Cambridge University Press; 2013, p. 357–60.

[39] Vaičaitis V, Butkus R, Balachninaitė O, Morgner U, Babushkin I. Diffraction-enhanced femtosecond white-light filaments in air. Appl Phys B 2018;124(11):221. http://dx.doi.org/10.1007/s00340-018-7090-y.

[40] Nurhuda M, Suda A, Hatayama M, Nagasaka K, Midorikawa K. Propagation dynamics of femtosecond laser pulses in argon. Phys Rev A 2002;66(2):023811. http://dx.doi.org/10.1103/PhysRevA.66.023811.